Slope stability assessment in sensitive clay with an advanced constitutive model

Proceedings 10th NUMGE 2023
10th European Conference on Numerical Methods in Geotechnical Engineering
Zdravkovic L, Kontoe S, Taborda DMG, Tsiampousi A (eds)

https://doi.org/10.53243/NUMGE2023-298

Slope stability assessment in sensitive clay with an advanced constitutive model

C. Sellin[1], M. Karstunen[1]

[1]*Department of Architecture and Civil Engineering, Chalmers University of Technology, Gothenburg, Sweden*

ABSTRACT: The initial and strain-induced anisotropic structure, as well as the strain-softening behaviour, of sensitive clay has been long recognized. These soil features, and their subsequent effect on the mobilized strength, are however rarely directly considered in the evaluation of slope stability. This numerical study investigates the influence of 1) Initial anisotropy; 2) Evolving anisotropy and 3) Degradation of the inter-particle bonds (destructuration) due to irrecoverable creep strains on the stability and failure mechanisms of a slope in sensitive clay. The rate-dependent Creep-SCLAY1S model includes these features, and its hierarchical formulation, is exploited to illustrate the effect of these features for a typical slope in the Göta River valley, West Sweden.

Keywords: mobilisation of shear strength; slope stability; fabric anisotropy; rate dependence; constitutive modelling

1 INTRODUCTION

The hydromechanical response of intact natural clays is partially governed by rate-dependency (e.g. Berre and Bjerrum, 1973, Graham et al., 1983, Li, 2019), and partially by an evolving structure (e.g. Burland, 1990, Birmpilis et al., 2022). In the case of sensitive clay, the latter origins from the gravitational sedimentation in sea or brackish water, followed by isostatic uplift and subsequent leaching, which has resulted in an anisotropic meta-stable structure. This structure consists both of a geometrical arrangement of particles and their contacts, here called fabric, and the bonds acting between these particles (Quigley and Thompson, 1966). The particles re-arrange during irrecoverable loading, resulting in changes in anisotropy and thereby also an evolving strength mobilisation. As a result of the inter-particle bonds, the sensitive clays behave relatively stiff until yielding, followed by a sudden bond degradation, called destructuration (Leroueil and Vaughan, 1990), with a characteristic strain-softening response.

These rate- and stress-path-dependent soil characteristics are important aspects when simulating geotechnical problem, but are rarely included in slope stability assessment. This could potentially lead to under- or overestimations of the stability, in particular when pore pressure changes attributed to climate change-induced scenarios should be accounted for.

This paper applies an effective stress-based, rate-dependent, anisotropic soil model with destructuration in slope stability assessment and investigates how these evolving soil properties affect the stability and the failure mechanism.

2 CONSTITUTIVE MODEL AND METHODOLOGY

Creep-SCLAY1S is a rate-dependent, hierarchical, extension of the Modified Cam Clay (MCC) model, which includes anisotropy, destructuration and Lode angle dependency (Gras et al., 2017, 2018, Sivasithamparam et al., 2015) developed at Chalmers University of Technology, Sweden. The model is commercially available in PLAXIS finite element software (PLAXIS bv., 2021), however the results presented here are based on the inhouse version.

Creep-SCLAY1S consists of three surfaces, as presented in Figure 1, which respectively represent an imaginary Intrinsic Compression Surface (ICS), a Current Stress Surface (CSS) and the border between small and large irrecoverable strain increments; a Normal Consolidation Surface (NCS).

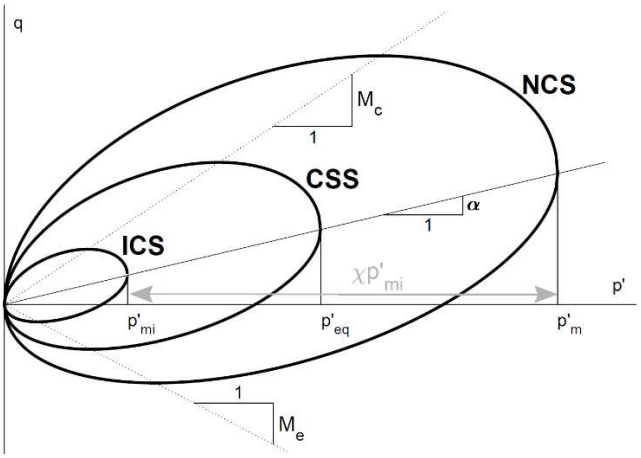

Figure 1. Definition of Creep-SCLAY1S in simplified triaxial space.

The concept of using an ICS (Koskinen et al., 2002) stems from Gens and Nova (1993), where an intrinsic surface mirrors an unbonded soil with the same void ratio and fabric orientation as its bonded equivalent.

The size of the three surfaces is determined by the intrinsic isotropic pre-consolidation pressure, p'_{mi}, the equivalent mean effective stress, p'_{eq}, and the isotropic preconsolidation pressure, p'_{m}, respectively, and the shape is governed by the stress ratio at critical state in compression (M_c) and extension (M_e), respectively. Notably, the generalized overconsolidation ratio p'_m/p'_{eq} governs the magnitude of the visco-plastic strains, see Grimstad et al. (2010), whereas the relation between p'_m and p'_{mi} describes the amount of bonding, χ, and any subsequent degradation of these bonds (Koskinen et al., 2002).

The orientation of the three surfaces in space is governed by the deviatoric fabric tensor, $\boldsymbol{\alpha}_d$, representing the fabric anisotropy, with a scalar equivalent α. The fabric anisotropy is defined by an initial value, α_0, and changes as a function of irrecoverable strains, resulting in a strain-dependent evolving anisotropy (Wheeler et al., 2003). The latter is described by a rotational hardening law:

$$\dot{\boldsymbol{\alpha}}_d = \omega \left[\left(\frac{3\boldsymbol{\sigma}'_d}{4p'} - \boldsymbol{\alpha}_d \right) \langle \dot{\varepsilon}_v^c \rangle + \omega_d \left(\frac{\boldsymbol{\sigma}'_d}{3p'} - \boldsymbol{\alpha}_d \right) \dot{\varepsilon}_d^c \right] \qquad (1)$$

where ω is the absolute rotational hardening, ω_d is the relative rate due to deviatoric strain, $\boldsymbol{\sigma}'_d$ is the deviatoric stress tensor and p' is mean effective stress. ε^c refers to the volumetric (v) and deviatoric (d) creep (c) strain respectively, and the Macaulay brackets, $\langle\ \rangle$, ensure only positive values of ε_v^c are affecting the rotation in the dry side, see Wheeler et al. (2003).

The inter-particle bonds and their degradation with respect to irrecoverable strains are similarly defined. The initial amount of bonding, χ_0, is reduced via a destructuration law (Koskinen et al., 2002). Notably, when the destructuration law is switched off, i.e. $\chi_0 = 0$, the ICS is not used and non-intrinsic model parameters should be used. For most cases, this affects only the modified (intrinsic) compression index, $\lambda^*_{(i)}$, since the modified creep index, μ^*, is equal to its intrinsic counterpart, μ_i^*, for sufficiently large stresses, when all bonds are erased (Gras et al., 2018).

The Lode-angle dependency is incorporated using the formulation by Sheng et al. (2000), modified to account for $\boldsymbol{\alpha}_d$, see Sivasithamparam et al. (2015).

When all features are activated, the Creep-SCLAY1S requires 14 model parameters. 11 of these are conventional (critical state) model parameters that can be derived from standard laboratory tests, and the remaining three are calibrated by triaxial test simulations, as shown in e.g. Amavasai et al. (2018) and Tornborg et al. (2021).

Most previous studies have started with a horizontal ground surface, which is actually a necessity for initialization of the model. That is due to the formulation of the deviatoric fabric tensor (Wheeler et al., 2003), which is defined in general stress space as:

$$\boldsymbol{\alpha}_d = \begin{bmatrix} \alpha_x - 1 \\ \alpha_y - 1 \\ \alpha_z - 1 \\ \sqrt{2}\alpha_{xy} \\ \sqrt{2}\alpha_{yz} \\ \sqrt{2}\alpha_{zx} \end{bmatrix} \qquad (2a) \qquad \alpha^2 = \frac{3}{2}\{\boldsymbol{\alpha}_d\}^T\{\boldsymbol{\alpha}_d\} \qquad (2b)$$

with the property:

$$\frac{\alpha_x + \alpha_y + \alpha_z}{3} = 1 \qquad (3)$$

This means that an arbitrary soil stratigraphy and ground surface geometry would require six parameters for describing the fabric rotation. To circumvent this for the case of slopes, where y-axis is vertical, the first calculation stage assumes a horizontal ground surface ($\alpha_{xy} = \alpha_{yz} = \alpha_{zx} = 0$) with cross-anisotropy ($\alpha_x = \alpha_z$) originating from 1D stress history, simulating the early origin of a natural slope with 1D sedimentation and isostatic uplift. $\boldsymbol{\alpha}_d$ can then be simplified to:

$$\boldsymbol{\alpha}_d = \left[-\frac{1}{3}\alpha_0 \quad \frac{2}{3}\alpha_0 \quad -\frac{1}{3}\alpha_0 \quad 0 \quad 0 \quad 0 \right]^T \qquad (5)$$

where α_0 can be derived from the critical friction angle via M_c and by applying Jaky's formula (Jaky, 1948), see Wheeler et al. (2003).

The intended slope geometry is then obtained by a simultaneous unloading, and dewatering in sufficiently small increments, until the final geometry and pore pressure distribution of the natural slope is obtained, as illustrated in Figure 2.

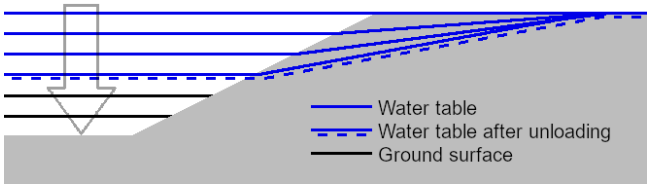

Figure 2 Illustration of the simultaneous unloading and ground water lowering to initialize the stress distribution.

The slope is then brought to failure by applying a gravitational increase (Chen and Mizuno, 1990), similar to a centrifuge test, since the evolving rate-dependent strength resulting from the model depends on the stiffness as well as the ultimate strength parameters. The results presented in this paper uses PLAXIS 2D (version 21.01.00.479) with the built-in linear increase of

gravity. The rate was chosen to 1-g per 12 h, with a maximum target value of 2-g. Such a high rate means that the failure is triggered by excess pore pressures, simulating the undrained situation.

3 BENCHMARK SLOPE

A representative geological site with large deposits of sensitive soft clay was chosen to illustrate the effect of fabric and bonding in the soil. The site is located 13 km north of Gothenburg, in the Göta River valley, and was extensively investigated during the planning and design process of BanaVäg i Väst with new motorway and highspeed railway in the area, see Karlsson and Karstunen (2017). The slope geometry and laboratory tests on samples from the site were used for calibration of the model parameters for Creep-SCLAY1S, with the resulting values presented in Table 1 and 2. The chosen values are further described in Sellin et al. (2023).

Table 1. Model parameters for Creep-SCLAY1S for the geological site.

Parameter	Definition	Value
λ_i^*	Modified intrinsic compression index	0.08
λ^*	Modified compression index	0.2
κ^*	Modified swelling index	0.008
ν'	Poisson's ratio	0.2
M_c	Stress ratio at critical state in triaxial compression	1.75
M_e	Stress ratio at critical state in triaxial extension	1.2
α_0	Initial value of anisotropy	0.72
ω	Absolute rate of rotational hardening	55
ω_d	Relative rate of rotational hardening	0.98
ξ	Absolute rate of destructuration	8
ξ_d	Relative rate of destructuration	0.35
χ_0	Initial amount of bonding	15
$\mu_{(i)}^*$	Modified (intrinsic) creep index	0.0013
τ	Reference time [days]	1

Table 2. Depth-dependent model parameters for the geological site.

Depth [m]	γ [kN/m³]	k_h=k_v [m/s]	OCR [-]	POP [kN/m²]	e_0
0 - 1.0	17.0	$1\cdot10^{-9}$	1.5	-	1.70
1.0 - 4.5	15.4	$1\cdot10^{-9}$	1.5	-	1.70
4.5 - 11.5	15.4	$8\cdot10^{-10}$	-	16.0	1.70
11.5 - 23.5	16.0	$8\cdot10^{-10}$	-	16.0	1.62
23.5 - 25.0	16.3	$6\cdot10^{-10}$	-	18.5	1.78

3.1 Isotropic model

First, an isotropic reference calculation was performed, where both fabric anisotropy and any degradation of bonds were excluded ($\alpha_0 = \omega = \chi_0 = 0$). The reference calculation thereby consists of a rate-dependent and Lode-angle dependent MCC-formulation, illustrated in Figure 3 using the mean effective stress, p', and the deviatoric stress, q.

The initialization of the stresses in the slope resulted in large stress rotations under the riverbed and in the lower part of the slope, as expected and shown in Figure 4.

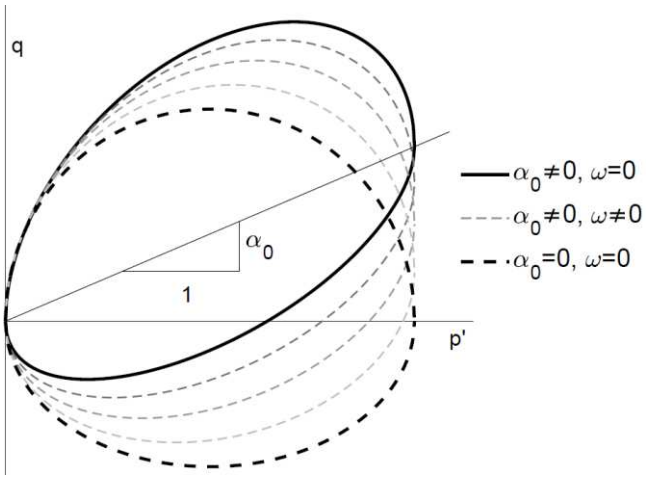

Figure 3. Surface rotation due to the deviatoric fabric tensor $\boldsymbol{\alpha_d}$, with an initial value of α_o.

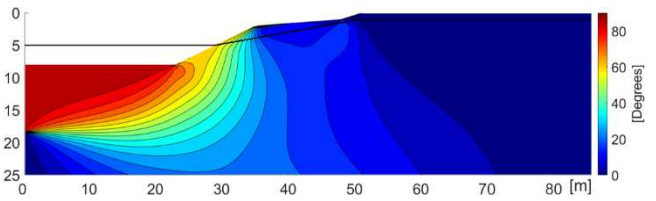

Figure 4 Principal stress directions, isotropic reference case.

This implies that strain-rate dependent mobilised strength will vary within the slope, as the real behaviours would be expected to be. However, when the gravitational increase is simulated using the isotropic model, the slope does not develop a failure mechanism for the 2-g/24 h loading, and total (imaginary) displacements up to 15 cm is predicted. The displacements occurred mainly at the toe of the slope, indicating a very localised movement. The results are expected, due to the significant overestimation of the mobilized strength in extension by an isotropic model compared to its anisotropic counterpart.

The same calculation setup was performed with inclusion of destructuration ($\alpha_0 = \omega = 0,\ \chi_0 \neq 0$). Since the destructuration only affects post-peak strength, the results show the same type of soil response, with maximum 15 cm of total displacement at the toe of the slope. The colour shadings in Figure 5 shows the size and distribution of the total displacement in the slope after gravitational increase.

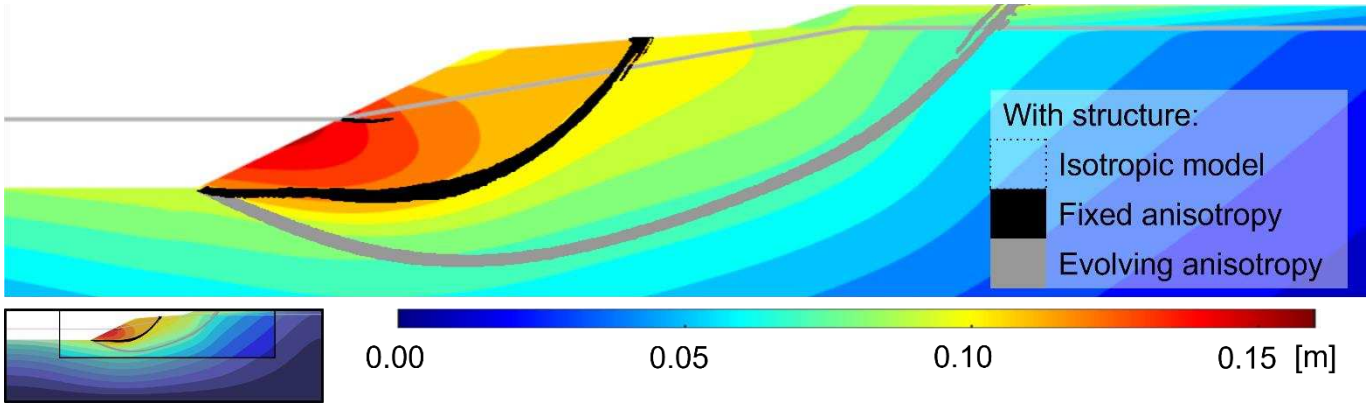

Figure 5 Colour shading represents total displacement for the isotropic reference calculation with destructuration. Black and grey failure lines illustrate the total deviatoric strains from calculations with fixed and evolving anisotropy, respectively.

3.2 *Effect of fixed anisotropy*

The initial rotation of the three surfaces, α_0, originates from the initialization of the model and the fabric orientation assuming horizontal ground surface, and represents the vertical sedimentation of clay particles. By assigning $\omega = 0$ in Eq. 1, this initial fabric rotation is fixed and unaffected by the subsequent irrecoverable strains from unloading. Thus, only initial anisotropy is considered and assumed to be fixed. Figure 3 illustrates this initial rotation with α_0 and its difference to the isotropic case. It should be noted that, given the Lode-angle dependency is included, the reference surfaces have a non-symmetrical shape around the α_0-axis.

A calculation was performed with fixed anisotropy and destructuration ($\alpha_0 \neq 0, \omega = 0, \chi_0 \neq 0$), which resulted in a failure after 8 h, corresponding to 0.66-g. Figure 5 shows the failure mechanism with respect to total deviatoric strains and, notably, a beginning of a second, much smaller, shear band in the middle of the slope.

The failure mechanism has a non-circular shape, as a result of the fixed anisotropy. Additionally, the mobilized strength is potentially overestimated in the upper part of the slope and is likely underestimated closer to the slope toe, as illustrated in Figure 3.

3.3 *Effect of evolving anisotropy*

Inclusion of the rotational hardening law (Eq. 1) allows the three surfaces to rotate in space, and thereby simulate the soil response under an evolving fabric anisotropy due to irrecoverable strains individually in each stress integration point. As a result, the initialized stresses in the slope, due to unloading and dewatering, are accounted for in this anisotropic formulation, and the anisotropy varies within the slope. The evolving rotation in one stress point is schematically illustrated in Figure 3, and the corresponding spatial variation of the scalar value of α is shown in Figure 6.

For the case of evolving anisotropy with destructuration ($\alpha_0 \neq 0, \omega \neq 0, \chi_0 \neq 0$), the gravitational increase results in a large failure mechanism, as depicted in Figure 5. The failure occurs after 17 h, corresponding to 1.40-g.

As seen, the slip surface is clearly larger than the corresponding slip surface using a fixed anisotropy, resulting in a more circular shape. Previous studies of the same slope (Sellin, 2019) using Tresca failure criterion has shown similar size and shape of the failure mechanism.

3.4 *Effect of destructuration*

The isotropic reference case did not develop a failure surface neither with nor without destructuration, and both the magnitude of the displacements and its pattern in the slope were very similar. This shows that the effect of destructuration is neglectable in slope stability context when no failure mechanism is developed, since the post-peak values are never reached.

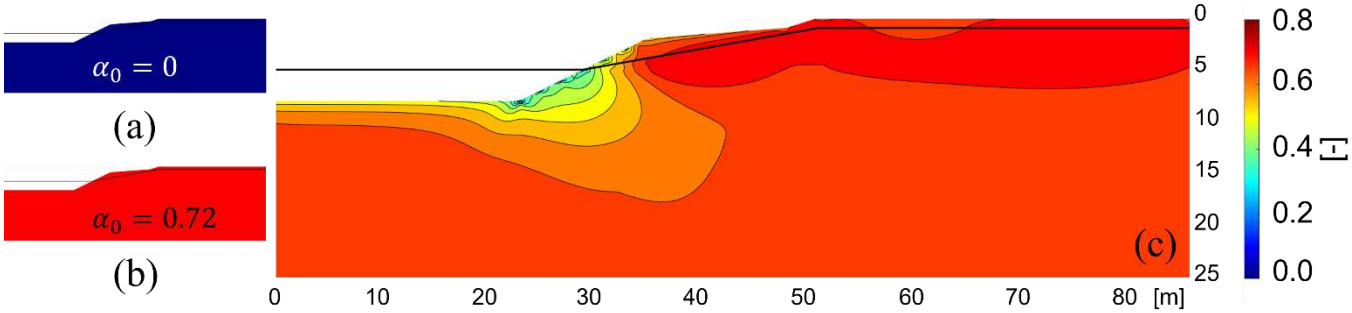

Figure 6 Scalar value of $\boldsymbol{\alpha}_d$ after slope formation; (a) isotropic model; (b) fixed anisotropy and (c) evolving anisotropy.

For the case with evolving anisotropy, the exclusion of destructuration ($\alpha_0 \neq 0, \omega \neq 0, \chi_0 = 0$) resulted in a wider shear band, as shown in Figure 7. The failure occurred after 22 h (at 1.85-g), clearly exceeding the stability obtained *with* destructuration. Same behaviour was noticed for the fixed anisotropy with/without destructuration, where the exclusion of destructuration resulted in a failure after 10 h (at 0.86-g). In the latter case, however, the failure mechanism changed shape to resemble the case with evolving anisotropy, as shown in Figure 7. This illustrates how the inclusion of post-peak softening, via the destructuration, affects the progression of the failure, the failure mechanism and thereby also the ultimate load that the slope can withstand.

Figure 7. Failure surfaces, here represented as total deviatoric strains, from simulations without destructuration.

4 CONCLUSIONS

The aim of the study was to investigate the use of an advanced constitutive model for slope stability assessment in sensitive clay via a benchmark slope. The hierarchical rate-dependent model used allows for isolation of the effects from fabric orientation and inter-particle bonds, respectively, on the stability and failure mechanism. The results show that the stability of a natural slope is overestimated when excluding anisotropy. Additionally, the use of a fixed anisotropy is likely to underestimate the mobilized strength in the lower, unloaded, part of the slope, and with both the failure mechanism and the ultimate gravity at failure (that can be considered as a proxy to the safety factor) varying with the use of destructuration.

When evolving anisotropy is included, the failure mechanism (in undrained conditions) is identical to previous studies of the slope using total stress analysis. The impact of destructuration is neglectable for the failure mechanism when using evolving anisotropy, but increases the ultimate gravity at failure, implying that the destructuration, as a fundamental feature of sensitive clay behaviour, affects the progression of the failure. The results highlight the importance of including evolving anisotropy and destructuration when simulating slope stability in sensitive soil using a rate-dependent model, in order to account for the spatially varying stress distribution and the corresponding soil response. The inclusion of rate-dependency ultimately allows for modelling the soil response as a function of time, enabling to account for environmental changes, such as changing pore pressures.

5 ACKNOWLEDGMENTS

Financial support from the Swedish Transport Administration in the framework of BIG (Branschsamverkan i Grunden, A2020-09), NordForsk (#98335) and the Swedish Research Council FORMAS (2021-02400) is greatly appreciated. The work is done as part of Digital Twin Cities Centre that is supported by Sweden's Innovation Agency VINNOVA.

6 REFERENCES

Amavasai, A., Sivasithamparam, N., Dijkstra, J., Karstunen, M. 2018. Consistent Class A & C predictions of the Ballina test embankment. *Computers and Geotechnics* **93**, 75–86.

Berre, T., Bjerrum, L. 1973. Shear strength of normally consolidated clays. *Proceedings of the 8th International Conference on Soil Mechanics and Foundation Engineering*, 39–49.

Birmpilis, G., Andò, E., Stamati, O., Hall, S. A., Gerolymatou, H. E., Dijkstra, J. 2022. Experimental quantification of 3D deformations in sensitive clay during stress-probing. *Géotechnique*, Advance online publication.

Burland, J. B. 1990. On the compressibility and shear strength of natural clays. *Géotechnique* **40**, 329–378.

Chen, W. F., Mizuno, E. 1990. *Nonlinear analysis in soil mechanics: Theory and implementation,* Elsevier, Amsterdam.

Gens, A., Nova, R. 1993. Conceptual bases for a constitutive model for bonded soils and weak rocks. Prof. International Symposium on Hard Soils- Soft Rocks (Eds: Anagnostopoulos, A., Schlosser, F., Kalteziotis, N. & Frank, R.), 485-494. A A Balkema, Rotterdam.

Graham, J., Crooks, J. H. A., Bell, A. L. 1983. Time effects on the stress-strain behaviour of natural soft clays. *Géotechnique* **33**, 327–340.

Gras, J.P., Sivasithamparam, N., Karstunen, M., Dijkstra J. 2017. Strategy for consistent model parameter calibration for soft soils using multi-objective optimisation. *Computers and Geotechnics* **90**, 164–175.

Gras, J.P., Sivasithamparam, N., Karstunen, M., Dijkstra J. 2018. Permissible range of model parameters for natural fine-grained materials. *Acta Geotechnica* **13**, 387–398.

Grimstad, G., Degago, S.A., Nordal, S., Karstunen, M. 2010. Modeling creep and rate effects in structured anisotropic soft clays. *Acta Geotechnica* **5**, 69–81.

Jaky, J.1948. Pressure in silos. *Proceedings of the 2nd International Conference on Soil Mechanics and Foundation Engineering*, 103–107.

Karlsson, M., Karstunen, M. 2017. On the benefits of incorporating anisotropy in stability analyses in sensitive clays. *Landslides in sensitive clays: from research to implementation* (Eds: Thakur, V., L'Heureux, J.S. & Locat, A.), 259-266. Springer International Publishing, Cham.

Koskinen, M., Karstunen, M., Wheeler, S.J. 2002. Modelling destructuration and anisotropy of a natural soft clay. Proceedings of the 5th European Conference on Numerical Methods in Geotechnical Engineering, (Eds: Mestat, P.), 11-20. Presses de l'ENPC, Paris.

Leroueil, S., Vaughan, P. R. 1990. The general and congruent effects of structure in natural soils and weak rocks. *Géotechnique* **40**, 467–488.

Li, Y. 2019. *On the impact of temperature perturbations on the creep of sensitive clay*, PhD thesis, Chalmers University of Technology, Gothenburg.

PLAXIS bv. 2021. PLAXIS CONNECT Edition V21.01 General information manual (Eds: Brinkgreve, R. B., Kumarswamy, S., Swolfs, W. M., Fonesca, F., Ragi Manoj, N., Zampich, I. & Zalamea, N.). Bentley Systems.

Quigley, R.M., Thompson, C.D. 1966. The fabric of anisotropically consolidated sensitive marine clay. *Canadian Geotechnical Journal* **3**, 61–73.

Sellin, C. 2019. On evaluating slope stability in sensitive clay -a comparison of methods through a case study. *Proceedings of the 27th European Young Geotechnical Engineers Conference* (Eds: Ülgen, D., Saygili, A., Kahyaoğlu, M.R., Durmaz, S., Toygar, O. & Göçügenci, A.), 249-254. Turkish Society for ISSMGE.

Sellin, C., Karlsson, M., Karstunen, M. 2023. Impact of rate-dependency on slope stability in sensitive clays. *Submitted manuscript.*

Sheng, D., Sloan, S. W., Yu, H. S. 2000. Aspects of finite element implementation of critical state models. *Computational Mechanics*, **26**, 185–196.

Sivasithamparam, N., Karstunen, M., Bonnier, P. 2015. Modelling creep behaviour of anisotropic soft soils. *Computers and Geotechnics* **69**, 46–57.

Tornborg, J., Karlsson, M., Kullingsjö, A., Karstunen, M. 2021. Modelling the construction and long-term response of Göta Tunnel. *Computers and Geotechnics* **134**, 104027.

Wheeler, S.J., Näätänen, A., Karstunen, M., Lojander, M. 2003. An anisotropic elastoplastic model for soft clays. *Canadian Geotechnical Journal* **40**, 403–418.